Biochimica et Biophysica Acta 1840 (2014) 626–636

Contents lists available at ScienceDirect

Biochimica et Biophysica Acta

journal homepage: www.elsevier.com/locate/bbagen

Mutation of a pH-modulating residue in a GH51 α-L-arabinofuranosidase leads to a severe reduction of the secondary hydrolysis of transfuranosylation products☆

Bastien Bissaro [a,b,c], Olivier Saurel [a,d], Faten Arab-Jaziri [a,b,c], Luc Saulnier [e], Alain Milon [a,d], Maija Tenkanen [f], Pierre Monsan [a,b,c], Michael J. O'Donohue [a,b,c], Régis Fauré [a,b,c,*]

[a] Université de Toulouse; INSA, UPS, INP; LISBP, 135 Avenue de Rangueil, F-31077 Toulouse, France
[b] INRA, UMR792, Ingénierie des Systèmes Biologiques et des Procédés, F-31400 Toulouse, France
[c] CNRS, UMR5504, F-31400 Toulouse, France
[d] CNRS, IPBS UMR 5089, Institut de Pharmacologie et de Biologie Structurale, 205 route de Narbonne, BP 64182 Toulouse, France
[e] UR1268 Biopolymères Interactions Assemblages, INRA, 44300 Nantes, France
[f] Department of Food and Environmental Sciences, Faculty of Agriculture and Forestry, University of Helsinki, P.O. Box 27, FI-00014, Finland

ARTICLE INFO

Article history:
Received 10 June 2013
Received in revised form 23 September 2013
Accepted 4 October 2013
Available online 17 October 2013

Keywords:
Pentoses/furanoses
Transglycosylation
pK_a modulation
pH-dependent inhibition
STD NMR

ABSTRACT

Background: The development of enzyme-mediated glycosynthesis using glycoside hydrolases is still an inexact science, because the underlying molecular determinants of transglycosylation are not well understood. In the framework of this challenge, this study focused on the family GH51 α-L-arabinofuranosidase from *Thermobacillus xylanilyticus*, with the aim to understand why the mutation of position 344 provokes a significant modification of the transglycosylation/hydrolysis partition.
Methods: Detailed kinetic analysis (k_{cat}, K_M, pK_a determination and time-course NMR kinetics) and saturation transfer difference nuclear magnetic resonance spectroscopy was employed to determine the synthetic and hydrolytic ability modification induced by the redundant N344 mutation disclosed in libraries from directed evolution.
Results: The mutants N344P and N344Y displayed crippled hydrolytic abilities, and thus procured improved transglycosylation yields. This behavior was correlated with an increased pK_a of the catalytic nucleophile (E298), the pK_a of the acid/base catalyst remaining unaffected. Finally, mutations at position 344 provoked a pH-dependent product inhibition phenomenon, which is likely to be the result of a significant modification of the proton sharing network in the mutants.
Conclusions and general significance: Using a combination of biochemical and biophysical methods, we have studied *Tx*Abf-N344 mutants, thus revealing some fundamental details concerning pH modulation. Although these results concern a GH51 α-L-arabinofuranosidase, it is likely that the general lessons that can be drawn from them will be applicable to other glycoside hydrolases. Moreover, the effects of mutations at position 344 on the transglycosylation/hydrolysis partition provide clues as to how *Tx*Abf can be further engineered to obtain an efficient transfuranosidase.

1. Introduction

So far, very few studies have dealt with the development of furanoside hydrolases (FHs) as glycosynthetic tools, with most work being performed on hexose and/or pyranose-acting enzymes [2–5]. This is unsurprising since, not only are FHs a relatively small subgroup of glycoside hydrolases (GHs), but also furanose chemistry is not a mainstream topic, in part because furanosides are often tricky to handle. Nevertheless, furanoses are quite widespread in Nature, being found in the cell wall polysaccharides of most plants and those of a variety of pathogenic microorganisms. Therefore, the development of chemo-enzymatic tools and methods is a pertinent pursuit, notably in the context of the production of new furanose-based products for a whole

Abbreviations: Abfs, α-L-arabinofuranosidases; AXOS, arabinoxylo-oligosaccharides; D-Xylp, D-xylopyranosyl; FH, furanoside hydrolase; GH, glycoside hydrolase; KIE, kinetic isotope effects; L-Araf, L-arabinofuranosyl; 4NTC-α-L-Araf, 4-nitrochatecol α-L-arabinofuranoside; *m*NP, *meta*-nitrophenol; *o*NP, *ortho*-nitrophenol; *p*NP, *para*-nitrophenol; *p*NP-α-L-Araf, *para*-nitrophenyl α-L-arabinofuranoside; R_T, transfer rate; STD NMR, Saturation Transfer Difference Nuclear Magnetic Resonance; T/H ratio, transglycosylation/hydrolysis ratio; *Tx*Abf, α-L-arabinofuranosidase from *Thermobacillus xylanilyticus*; *Tx*Abf$^+$, inactivated form (E176A) of *Tx*Abf; X, donor conversion rate; Y, yield

☆ The specific abbreviated names of different AXOS, such as A^3X and XA^3XX, were generated using the naming system developed by Fauré et al. [1].

* Corresponding author at: Laboratoire d'Ingénierie des Systèmes Biologiques et des Procédés, 135 Avenue de Rangueil, 31077 Toulouse cedex 4, France. Tel.: +33 5 6155 9488; fax: +33 5 6155 9400.
E-mail address: regis.faure@insa-toulouse.fr (R. Fauré).

0304-4165/$ – see front matter © 2013 Elsevier B.V. All rights reserved.
http://dx.doi.org/10.1016/j.bbagen.2013.10.013

range of applications, from tailored oligo- and polysaccharides and alkyl-polypentosides [6], to the synthesis of furanose-based glycomotifs for therapeutic purposes [7–9].

Whichever the GH under study, the key challenge associated with the use of these enzymes as glycosynthetic tools is competition with hydrolysis, which is an intrinsic and usually dominant activity of GHs. In this respect, thermodynamically-favorable hydrolysis competes with glycosynthesis at two stages. First, the two reactions compete for the donor substrate, with the outcome being either hydrolysis or glycosynthesis, and then, if synthesis occurs, hydrolysis intervenes again upon product accumulation, causing the decomposition of the transglycosylation product and thus a reduction of its final yield. To address this challenge, several approaches have been developed, with glycosynthases being a well-studied example. Glycosynthases are GHs that have been rendered catalytically-impotent through the elimination of the catalytic nucleophilic residue [10]. Only in the presence of highly-activated (generally 1-fluorosyl) donor glycosides, can glycosynthases mediate synthesis [4]. Moreover, once the donor glycoside is transferred onto an acceptor by a glycosynthase, the resulting product cannot be hydrolyzed. However, the fact that glycosynthases require glycosyl fluoride donors severely limits their application in the area of FHs, due to the extreme instability of furanosyl 1-fluorides.

Alternative strategies to create GH-based transglycosidases include directed evolution approaches that implement various screening protocols to select for GHs that better catalyze transglycosylation and/or perform less hydrolysis. So far, although these experiments, which rely on random mutagenesis, have provided a variety of interesting observations, but taken together they have not yet provided any generic engineering rules for the improvement of the transglycosylation potency [11–23].

The modulation of the transglycosylation/hydrolysis (T/H) ratio via the modification of reactions conditions (e.g. increasing reactant concentrations [24,25], changing the operating temperature [26] or pH [27–30], or the use of a co-solvent [31]) is also an option that has been studied to promote GH-mediated glycosynthesis.

In retaining GHs, hydrolysis (and transglycosylation) operates via a double displacement mechanism that is catalyzed by two acidic residues (aspartate or glutamate), one acting as the general acid/base and the other as the nucleophile (Fig. 1). Therefore, since GH activity depends on the pK_a of the catalytic residues, 'pK_a cycling' during the reaction has been the subject of several careful analyses [32–38] and a recent report has provided significant insight into how residues that surround the catalytic dyad can influence this process [39]. Nevertheless, precise generic rules to identify the factors that determine the ionization states of the nucleophile and acid/base catalytic residues and, more generally, the catalytically-pertinent electrostatic interactions within GHs, remain elusive. Therefore, rational engineering aimed at modifying the optimum pH of GHs is not yet feasible. Moreover, it is noteworthy that the impact of modifications of the pK_a of catalytic residues in GHs on transglycosylation has never been addressed.

The glycosynthetic properties of the GH51 α-L-arabinofuranosidase from *Thermobacillus xylanilyticus* (*Tx*Abf) have been extensively described, making this enzyme a paradigm for FH-mediated transglycosylation [40–44]. In recent work, we have adopted a directed evolution approach in an attempt to modulate the T/H ratio, using a high-throughput assay to select *Tx*Abf variants that display higher

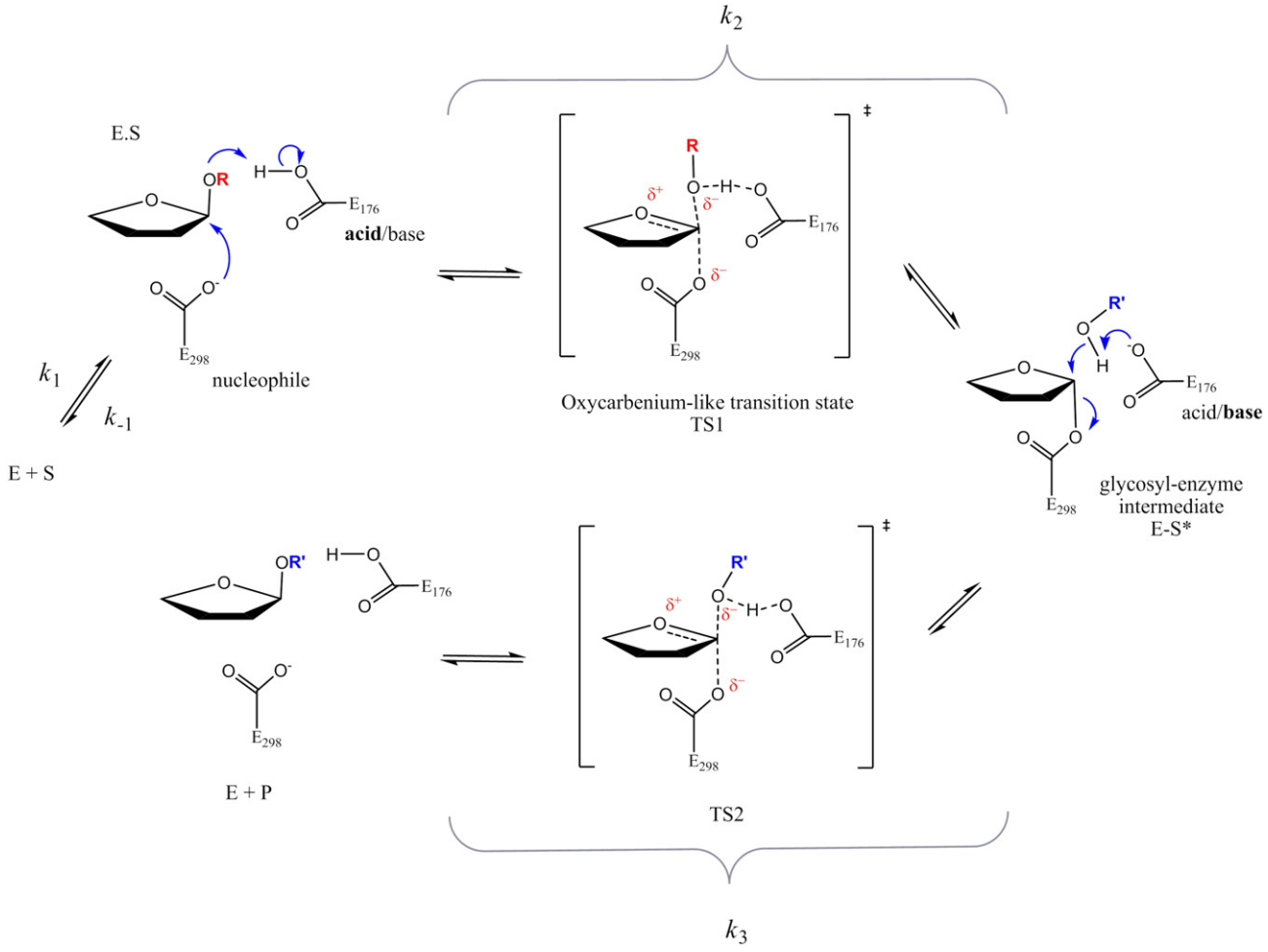

Fig. 1. Schematic representation of *Tx*Abf-catalyzed reactions through the double displacement mechanism of retaining GHs (R = leaving group and R′ = xylobiosyl, xylotriosyl for transglycosylation or H for hydrolysis).

activity in the presence of artificial or natural acceptor sugars. This work has provided a series of mutants, some of which display significantly lower levels of primary and secondary hydrolysis when compared to the wild type enzyme [44,45]. Among the mutations that have been detected, we observed that the residue N344 was quite often subject to substitution. Therefore, in our present study, we have performed a thorough characterization of a library of N344 mutants, which has allowed us to offer a detailed description of the impact on hydrolytic and transglycosylation activities of mutations at this position.

2. Materials and methods

2.1. Substrates and chemicals

Unless otherwise stated, routine experimental work was performed using chemicals purchased mainly from Sigma-Aldrich (Illkirch, France) and molecular biology reagents purchased from New England Biolabs (Evry, France). The substrate, *p*NP-α-L-Ara*f*, was prepared in-house according to established or adapted protocols [46,47]. The AXOS, A^3X and XA^3XX, were isolated and purified as previously described [48,49]. Xylotriose and XOS, used as acceptors, were purchased from Wako Chemicals GmbH (Neuss, Germany). Xylobiose was prepared in-house as previously described [50], using XOS as the starting material. ESI-HRMS: *m/z* calcd for $C_{10}H_{18}O_9Na$: $[M + Na]^+$ 305.0843; found: 305.0845 (1 ppm) [51].

2.2. Mutagenesis, protein expression, and purification

The plasmid construction pET24a-*Tx*Abf (original pET vectors from Novagen, Fontenay-sous-Bois, France) was used as template DNA for *in vitro* mutagenesis using the QuikChange Site-Directed Mutagenesis kit (Agilent, Courtaboeuf, France), following the manufacturer's instructions.

The asparagine residue present at position 344 (NNN = AAC) in the *Tx*Abf-encoding sequence (GenBank accession number CAA76421.2) was replaced by the 19 other amino acids using the following primers (underline letters represents mutated bases in NNN = AAC codon) for N344A (GCG), N344C (TGC), N344D (GAT), N344E (GAA), N344F (TTC), N344G (GGC), N344H (CAT), N344I (ATT), N344K (AAA), N344L (CTG), N344M (ATG), N344P (CCG), N344Q (CAG), N344R (CGT), N344S (AGC), N344T (ACC), N344V (GTG), N344W (TGG), N344Y (TAT):

N344X 5′-CGCGTCCGGATGGCG**NNN**ATCGCCCAGCTCG-3′

For STD experiments, mutations at position 344 were combined with the mutation E176A, which led to the production of inactivated enzymes, hereafter denoted by the symbol '+' (e.g. $N344Y^+$). This mutation was achieved using the following primer:

E176A 5′-GGCGTCGGCAAC**GCC**AACTGGGGCTGC-3′

The successful introduction of mutations was confirmed by DNA sequencing (GATC Biotech, Mulhouse, France). Expression and subsequent purification of wild-type and mutated recombinant *Tx*Abf, produced in *E. coli* BL21(DE3), were performed as previously described [52]. Briefly, enzyme crude extracts were obtained by sonication of cell pellets on ice (Bioblock Scientific vibracell 72434), employing cycles of 0.5 s 'on', 1.5 s 'off' during 8 min, with the probe operating at 30% of maximal power. The cell extract was then heat-treated (75 °C, 30 min) and clarified using centrifugation (30 min at 11,000 ×*g*, 4 °C). Exploiting the presence of a C-terminal $(His)_6$ tag, *Tx*Abf and mutants thereof were purified using a Cobalt resin (TALON® Metal Affinity Resin, Clontech Laboratories, Inc.) contained in a disposable column (Bio-Spin column, Bio-Rad). Elution of recombinant proteins from the resin was achieved under gravity feed using a gradient of imidazole in TALON buffer (one volume each of 5 and 10 mM imidazole, followed by three volumes of 100 mM imidazole and finally one volume of 200 mM imidazole). Fractions were then analyzed using SDS-PAGE (Bio-Rad) and those containing purified enzyme were pooled and dialyzed overnight at 4 °C against Tris-HCl buffer (20 mM, pH 8) and stored at 4 °C.

2.3. Kinetic studies

Michaelis–Menten kinetic parameters K_M, k_{cat} and k_{cat}/K_M of *Tx*Abf and mutants thereof were determined using a discontinuous enzyme assay. Reactions were performed in duplicate at 45 °C in buffered conditions using *p*NP-α-L-Ara*f* (0.25–10 mM) and 0.1 $mg.mL^{-1}$ BSA. For buffering, sodium acetate buffer (50 mM) was used in the pH range 3.5–5.8, while sodium phosphate buffer (50 mM) was used to cover the pH range 5.8–9.0, with a common point being measured in both buffers at pH 5.8 for each enzyme and each substrate concentration. The total reaction volume was 400 μL and reactions were performed over a 10–20 min period, removing samples at regular intervals. Hydrolysis reactions were terminated by addition of 250 μL of sodium carbonate (1 M) to 50 μL of reaction mixture. After, absorbance at 401 nm was measured using a VersaMax microplate spectrophotometer and the quantity of *p*NP released was calculated using an appropriate standard curve, prepared using pure *p*NP. Negative controls containing all of the reactants except the enzyme were used to correct for spontaneous hydrolysis of the substrates. One unit (IU) of enzyme specific activity corresponds to the amount of enzyme releasing one μmol of *p*NP per minute. Appropriate enzyme quantities (in the nM range) were used in combination with suitable substrate concentrations, such that less than 10% of the total substrate was hydrolyzed over the course of the measurement. The pH of each assay solution was measured at the end of the reaction. Experimental initial rates were fitted to the standard Michaelis–Menten expression using SigmaPlot 11.0 software (Systat software Inc, Ritme, Paris, France), and k_{cat}/K_M data were plotted as a function of pH and fitted to a bell-shaped activity profile as described in Eq. (1) [37]. This analysis provided the apparent pK_a values corresponding to the nucleophile (pK_{a1}) and the acid/base (pK_{a2}) catalytic amino acids, which were determined by nonlinear least-squares fitting on Excel.

$$\frac{k_{cat}}{K_M} = \left(\frac{k_{cat}}{K_M}\right)_{max} \cdot \left(\frac{1}{1 + \frac{10^{-pH}}{10^{-pKa_1}} + \frac{10^{-pKa_2}}{10^{-pH}}}\right) \quad (1)$$

2.4. Monitoring transglycosylation

2.4.1. Thin layer chromatography screening

Analytical thin-layer chromatography (TLC — silica gel 60 F_{254} precoated plates, Merck) was used to qualitatively monitor reactions performed at optimal temperature, *p*NP-α-L-Ara*f* (5 mM) and Bn-α-D-Xyl*p* (5 mM). Reactions were stopped when the donor was fully consumed. TLC was achieved using an ethyl acetate/acetic acid/water (7:2:2, v/v/v) mobile phase and the migration profile was revealed using a UV lamp, following soaking in an orcinol solution (1 g in 1 L of sulphuric acid/ethanol/water solution, 3:72.5:22.5, v/v/v) and charring.

2.4.2. Time course NMR monitoring

Reactions were monitored by collecting ^1H NMR spectra using a Bruker Avance 500 spectrometer. First, the enzymatic solutions were diluted 10-fold in D_2O (99.90%) and then concentrated on an Amicon® Ultra filter (regenerated cellulose 10 kDa, Millipore), this operation being performed twice. The reference used was the residual water peak, calibrated at $\delta = 4.55$ ppm at 45 °C [53]. Transglycosylation reactions were performed at 45 °C, a temperature arbitrarily chosen to reflect a compromise between activity and stability. Reactions were

prepared in 600 μL of buffered D_2O (final volume), containing donor and acceptor at a ratio of either 1:1 (5 mM each) for Bn-α-D-Xyl*p*, or 1:2 (5 and 10 mM respectively) for xylobiose and xylotriose. Deuterated acetate (Euriso-Top, France) was used to prepare a buffer displaying a pD value of 5.9, while deuterated phosphate was used to attain a value of pD 7.1. Deuterated sodium phosphate was prepared in-house by dissolving sodium phosphate in D_2O, followed by lyophilisation. This two-step protocol was repeated three times to achieve sufficient deuteration. Values of pD were measured by determining pH using a glass pH electrode and then applying the equation $pD = pH_{electrode} + 0.41$ [54].

The amount of *Tx*Abf or mutant enzyme added was adjusted for each enzyme to achieve 0.05 IU (activity measured on *p*NP-α-L-Ara*f*, in D_2O at 45 °C), thus final enzyme concentrations were in the range 8–25 μM. ^1H NMR spectra were accumulated semi-continuously over 4 to 15 h by accumulating a series of 5.52 min scan periods (i.e. 32 scans) that were interspersed by delay periods of 6 s. The exact full monitoring period was dependent on the enzyme employed. Each NMR spectrum was acquired using an excitation flip angle of 30° at a radiofrequency field of 29.7 kHz, and the residual water signal was pre-saturated during the repetition delay (with a radiofrequency field of 21 Hz). The following acquisition parameters were used: relaxation delay (6 s), dummy scans (4). For each reaction, before enzyme addition, an NMR spectrum of the reaction mixture was acquired, serving as the starting point of the reaction, from which integrals were then corrected according to the small dilution factor induced by the enzyme addition (<5% of total volume).

2.4.3. NMR kinetics analysis

For data processing, the time-dependent evolution of donor (*p*NP-α-L-Ara*f*) and acceptor (Bn-α-D-Xyl*p*) concentrations were quantified by integrating the relative anomeric proton signal (5.85 and 4.98 ppm, respectively). Molar balances, based on acceptor and donor consumption, were used to convert the transglycosylation product signal integral (5.08 and 5.07 ppm for H-1 of α-L-Ara*f* and H-1 of α-D-Xyl*p*, respectively) into concentration, and to evaluate hydrolysis product concentrations, respectively. Moreover, agreement between acceptor and transglycosylation product integrals was also verified. In the case of xylobiose and xylotriose, signal overlapping excluded the possibility of performing reliable integrations. Consequently, as an alternative, first donor consumption was evaluated using the signals of five different entities: $H(pNP)_{meta}$ or $H(pNP)_{ortho}$ in the free state, released after *p*NP-α-L-Ara*f* hydrolysis (8.14 and 6.86 ppm, respectively) and linked forms (8.28 and 7.25 ppm, respectively) as well as from H-1 of *p*NP-α-L-Ara*f* (5.85 ppm). Since the sum of *p*NP (free and linked) remains constant throughout the reaction, this information was used as an internal standard to correlate the integral value to the initial concentration, independently for each spectrum, as follows:

$$I_{pNP,\ meta(free)} + I_{pNP,\ meta(linked)} = 2.I_{0,\ meta} \quad (2)$$

$$I_{pNP,\ ortho(free)} + I_{pNP,\ ortho(linked)} = 2.I_{0,\ ortho} \quad (3)$$

where I_0 corresponds to the integral of one proton at t_0 (initial concentration), and the sum of $I_{pNP,\ x}$ corresponds to $2.I_0$, since I_{pNP} integrates for two protons. A mean value for I_0 ($I_{0,\ mean}$) was calculated from $I_{0,\ meta}$ and $I_{0,\ ortho}$. Finally, the donor substrate conversion rate (X) can be calculated in three different ways from one spectrum as follows:

$$X_{meta}(\%) = \left(I_{pNP,\ meta(free)}/2.I_{0,\ meta} + I_{auto}/I_{0,\ mean}\right) * 100 \quad \text{(from Eq. 2)}$$

$$X_{ortho}(\%) = \left(I_{pNP,\ ortho(free)}/2.I_{0,\ ortho} + I_{auto}/I_{0,\ mean}\right) * 100 \quad \text{(from Eq. 3)}$$

$$X_{H-1}(\%) = \left(1 - I_{H-1}/I_{0,\ mean}\right) * 100$$

The donor conversion takes into account the consumption of the donor substrate toward hydrolysis and transglycosylation products, as well as self-condensation (I_{auto}). A mean conversion rate and the associated error are then deduced from the three previous values. For all time-course NMR kinetics, the absolute error mean value on X ranged between 1 and 3%.

Next, the transglycosylation yield was determined by integrating the signal of the anomeric proton of products (5.39, 5.32 and 5.27 ppm for XA^3X, A^3XX and A^2XX (or XA^3, A^3X and A^2X, respectively, when xylobiose was used as an acceptor) [48,55–59] and then dividing by $I_{0,\ mean}$, thus procuring a transglycosylation yield (Y): $Y_{(product)}(\%) = (I_{H\text{-}1(product)} / I_{0,\ mean}) * 100$. Finally, $Y_{(product)}$ (%) was plotted against X (%) to provide a transfer rate (R_T) of the donor substrate to a given product (μmoles of product/μmoles of consumed substrate), that is independent of the duration of the reaction (Supplementary Table 1 and Fig. 5). For each kinetics, the linear region for slope determination varied from X = 0–25% up to 0–40%, with root mean square deviations between 0.95 and 0.99.

2.5. STD NMR experiments

Samples were prepared in 600 μL of D_2O (5 mm NMR tubes) when *p*NP-α-L-Ara*f* (100 μM) was used as ligand, or in 170 μL of D_2O (3 mm NMR tubes) for A^3X (2 mM) or XA^3XX (2 mM), with a constant molar ratio of 1:100 (protein:ligand). STD NMR experiments were performed at 283 K with a Bruker Avance 600 spectrometer equipped with a cryoprobe TCi [60]. To achieve this, proteins were saturated on resonance at −0.4 ppm on methyl signals, and off resonance at 30 ppm, with selective Gaussian-shaped pulses of 50 ms duration, at a radio-frequency field of 86 Hz, with a 100 ms delay between each pulse. The total saturation time was 2 s. A WATERGATE sequence was used to suppress residual HOD signal. An identical experiment with no enzyme was used as a negative control in order to verify the selectivity of the saturation and the efficiency of the signal subtraction used to obtain the difference spectrum. Intensities of all STD effects (I_{STD}) were calculated by integration of the respective ^1H NMR signals and standardized with the reference signal I_0. The ratios of the intensities I_{STD}/I_0 were normalized using the largest STD effect (the H-3 proton of the L-Ara*f* unit was set to 100%) as a reference. In order to compare the impact of mutations on absolute STD effects, STD effects of protons exhibiting identical chemical shifts were standardized for each mutant, using the STD data obtained with *Tx*Abf. All data were acquired and processed using Topspin v2.1 software (Bruker).

3. Results

3.1. The impact of N344 mutations on transglycosylation

During the course of previous work involving the screening of randomly generated libraries of *Tx*Abf variants, five independent clones selected for their apparent ability to better perform transglycosylation were found to be mutated at position N344 [44,45]. The substitution N344Y occurred twice, while N344K, S and I were each found once. Interestingly, N344 is not directly located within the active site, but is rather found on strand β8 in the vicinity of the catalytic nucleophile E298 (β7 strand), within a zone that can be referred to as the second shell (Fig. 2). Examination of the conservation of N344 within GH51 family revealed that N344 is not a highly conserved residue, though 270 sequences (55%) do display this side-chain at an equivalent position. The next most frequent occurrences are cysteine (147 sequences or 30%) and serine (9%), which like asparagine also display electronegative character (Supplementary Fig. 1). The localization of N344 homologues in the structures of other GH51 Abfs showed that homologous asparagine residues are identically positioned in two Abfs of *Thermotoga* sp. origin (N323 for *Tm*Abf and *Tp*Abf, PDB ID: 3UG5 and 3S2C respectively), while homologous residues in Abfs from *Geobacillus stearothermophilus* (C348 in PDB ID: 1QW8), *Clostridium thermocellum* (C349 in PDB ID: 2C7F) or *Bifidobacterium longum* (S406 in PDB ID: 2Y2W) adopt similar, but not identical,

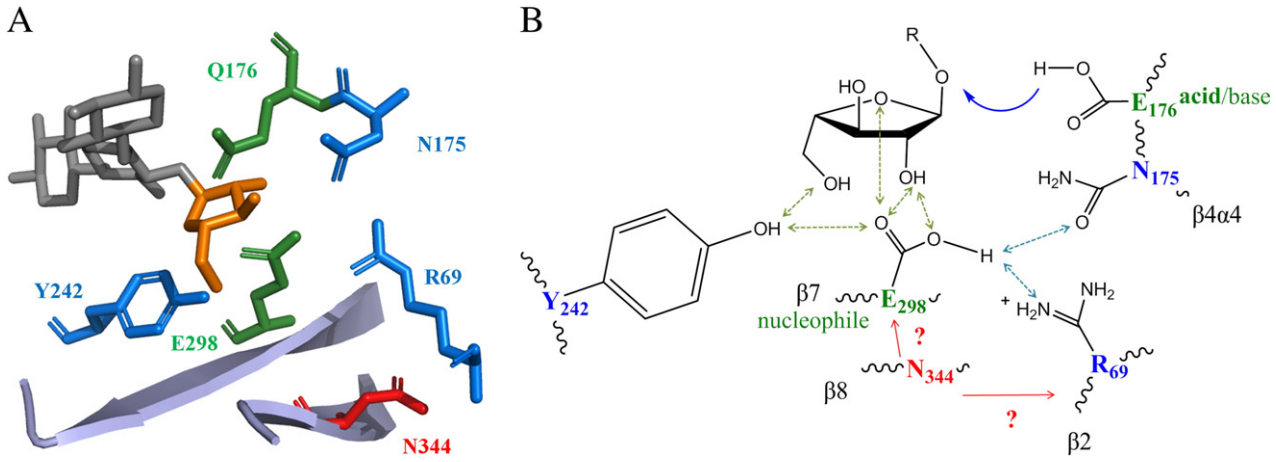

Fig. 2. View of the *Tx*Abf-XA^{3}XX complex active site. (A) N344 location relative to the inactivated *Tx*Abf-E176Q active site close to the catalytic nucleophile E298 and to the L-Ara*f* moiety in subsite −1 (PDB ID: 2VRQ) [66]; and (B) putative impact (red arrows) on hydrogen bonding (green and light blue) and electronic displacement system.

orientations and occupy similar steric volumes. Therefore, accounting for these observations and to further investigate the precise role of N344, notably with regard to its potential role in determining the partition between hydrolysis and transglycosylation, we created a site-saturation mutant library, which was then submitted to a variety of analyses.

To begin characterization of the nineteen position 344 mutants, a TLC-based assay was used to assess the ability of individual mutants to transfer an L-arabinofuranosyl (L-Ara*f*) donor moiety onto the acceptor, Bn-α-D-Xyl*p*. Indeed, it has been shown that *Tx*Abf can catalyze this reaction, forming Bn α-L-Ara*f*-(1,2)-α-D-Xyl*p* [40,44]. In our assay, six mutants (N344F, G, K, P, W and Y) displayed potentially higher yields than the reference reaction (13%), with three of these also displaying highly reduced secondary hydrolysis (N344G, P and Y). Therefore, using these preliminary results, the six improved mutants were selected for further analysis using time-course NMR, which confirmed our initial observations, revealing that the yield of transglycosylation product reached up to 20% in the case of N344K and 18% for N344Y or 15% for N344P and G (Supplementary Fig. 2). Moreover, whereas for N344K secondary hydrolysis was observed (similar to *Tx*Abf), in the case of N344P and Y, once synthesized, the amount of Bn α-L-Ara*f*-(1,2)-α-D-Xyl*p* remained stable for over 100 min, indicating that secondary hydrolysis was diminished to an undetectable level. The reaction catalyzed by the mutant N344G displayed a similar profile, although some secondary hydrolysis was evidenced. In this respect it is noteworthy that the thermostability of the six mutants was mostly unaffected, since all conserved >85% of residual activity after incubation for 4 h at 45 °C, thus confirming that reductions in primary and secondary hydrolysis were not due to heat denaturation. Finally, for the different mutants it was noted that for the donor/acceptor pair, *p*NP-α-L-Ara*f*/Bn-α-D-Xyl*p*, the transglycosylation product yield reached a stable endpoint, but donor consumption continued, although this was never complete, with 15% initial *p*NP-α-L-Ara*f* remaining at the end of the reaction for mutants N344P and Y.

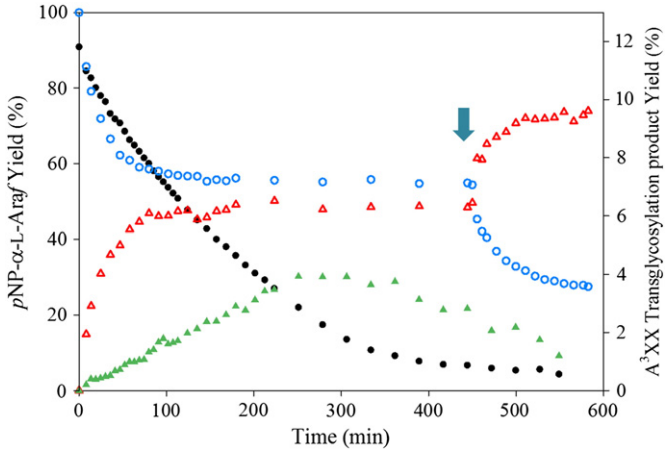

Fig. 3. Time-course NMR monitoring of A^{3}XX (5.32 ppm) transglycosylation product (▲ and △, for *Tx*Abf and N344Y respectively) obtained by transglycosylation reaction catalyzed by *Tx*Abf (8 nM) or N344Y (419 nM), with *p*NP-α-L-Ara*f* (5 mM) as donor (● or ○, respectively) and xylotriose (10 mM) as acceptor. An equal quantity of enzyme (419 nM) was added once steady state was reached (at t = 455 min, blue arrow). Assays were conducted in 25 mM deuterated acetate buffer (pD 5.9) at 45 °C.

Having revealed the improved transglycosylation ability of the six N344 mutants, N344G, P and Y were submitted to further tests in order to ascertain the ability of these mutants to catalyze the transfer of L-Ara*f* donor moieties onto xylobiose or xylotriose, taking into account the fact that when catalyzing such reactions parental *Tx*Abf procures quite low yields (10%) [45]. Like the previous analyses, time-course NMR revealed that the reactions attained a plateau after 100 min (Fig. 3) and quantification of products showed that N344P and N344Y procured higher yields compared to *Tx*Abf (Supplementary Table 1). Closer analysis of the products produced in each reaction revealed that four regio-isomers were formed in different proportions (Supplementary Fig. 3). Compared to reactions catalyzed by *Tx*Abf, those catalyzed by N344Y displayed increased yields (1.7-, 1.8- and 2.5-fold) of A^{3}XX (5.32 ppm), A^{2}XX (5.27 ppm) and XA^{3}X (5.39 ppm), respectively. It is noteworthy that because N344Y catalyzed the formation of XA^{2}X (5.28 ppm) [56,58] in quite negligible quantities, rather like parental *Tx*Abf, this particular reaction was not further analyzed. Furthermore, N344Y did display higher transfer rate, R_T, with increases reaching up to 4.6-fold compared to *Tx*Abf. Regarding N344K-catalyzed reactions performed in the presence of xylobiose or xylotriose, these provided maximum transglycosylation yields (Y_{max}) of up to 14% for A^{2}XX as opposed to *Tx*Abf (6%), associated with a 4.7-fold increase in the R_T.

3.2. Kinetic analysis of the hydrolytic activities of N344 mutants

According to the double displacement mechanism applied to retaining GHs, transglycosylation occurs at the deglycosylation step, and when donor substrates with good leaving groups are employed (i.e. $k_2 >> k_3$), $k_{cat} = k_2.k_3/(k_2 + k_3) \approx k_3$ (Fig. 1) [61–63]. Therefore, to investigate how mutations at position 344 might have altered the

Table 1
Steady-state kinetic parameters for the hydrolysis of *p*NP-α-L-Ara*f* by *Tx*Abf and N344P and Y mutants.

Enzyme	k_{cat}[a] (s^{-1})	K_M[a] (mM)	k_{cat}/K_M ($s^{-1}\,mM^{-1}$)	Relative k_{cat}/K_M	$pK_{a\ E298}$[b]	$pK_{a\ E176}$[b]	pH_{opt}[c]
*Tx*Abf	431 ± 10	0.27 ± 0.03	1671	100	4.6	7.6	6.1
N344P	81 ± 3	0.98 ± 0.13	81	4.8	6.1	7.8	7.0
N344Y	17 ± 0.6	0.63 ± 0.09	28	1.7	6.4	7.6	7.0

[a] k_{cat} and K_M values were measured at 45 °C, pH 5.8 (for *Tx*Abf) and pH 7.0 (for mutants N344P and Y).
[b] Apparent p*K*a were determined by fitting experimental values to the bell-shaped model shown in Fig. 4 (Eq. (1) from Section 2.3). The error on pK_a values is estimated to be 0.1 pH unit.
[c] pH_{opt} was determined as the value of the pH when the derivative of the model, to which experimental points were fitted, is equal to zero.

deglycosylation step, the kinetic parameters describing the hydrolysis of *p*NP-α-L-Ara*f* catalyzed by N344P and N344Y were determined in reactions buffered at the optimum pH (Table 1). As expected, this revealed that the k_{cat} values describing the two reactions were strongly decreased (81 and 96% for N344P and N344Y respectively), compared to the k_{cat} value of *Tx*Abf. Furthermore, the values of K_M were slightly raised and k_{cat}/K_M, or alternatively $k_1.k_2/(k_{-1} + k_2)$, reflecting the glycosylation step (enzyme-substrate association and glycosidic bond cleavage) was severely reduced (21 and 60-fold for N344P and Y respectively). Next, in order to better understand these results in terms of the electronic charge developed within the active site, the apparent pK_a values of the catalytic amino acids were determined by measuring the pH-dependency of the second order rate constant k_{cat}/K_M [37]. The data for *Tx*Abf and the two mutants were fitted to the bell-shaped model (Fig. 4), revealing summits at pH 6.1 (*Tx*Abf) and 7.0 (N344P and Y). Likewise, the data was found to be consistent with the presence of two ionizable groups, presumably corresponding to the catalytic acid/base (E176) and the nucleophile (E298), with apparent pK_a values for *Tx*Abf of 7.6 and 4.6, respectively. However, for the two mutants the apparent values of the lower pK_a were increased by >1 pH unit to 6.1 (N344P) and 6.4 (N344Y) respectively, while the more basic limbs of the pH-dependency profiles were mostly unaffected (7.8 and 7.6, respectively), with variations being considered to be within the error range (0.1 pH unit).

3.3. Solvent kinetic isotope effects

To further investigate the reactions catalyzed by the mutants N344P and Y, solvent kinetic isotope effects (KIE) were determined and compared to those of *Tx*Abf. These experiments revealed that the substitution of water hydrogen atoms by deuterium led to an increase of the ratio k_H/k_D, by only 4% for N344P and 37% in the case of N344Y (Supplementary Table 2). The wild-type solvent KIE value (1.88) reveals a modest impact of deuterium substitution, but is in agreement with other KIE values measured for other GHs [63,64].

3.4. pH optima for glycosynthesis

Taking into account the altered pH optimum of the mutants and the failure of external nucleophiles to rescue the reaction, the impact of the ionization state in the active site on transfer activity and secondary hydrolysis was investigated. To achieve this, time-course NMR was used to monitor both the consumption of *p*NP-α-L-Ara*f* and the production of transglycosylation products in comparable reactions catalyzed by N344P or Y, operating at pD 7.1 or pD 5.9. At pD 7.1, consumption of *p*NP-α-L-Ara*f* was complete within 100 min and evidence of secondary hydrolysis was detected, since the maximum yields of the transglycosylation products were not conserved over time (Fig. 5). In contrast, at pD 5.9, *p*NP-α-L-Ara*f* consumption was incomplete and secondary hydrolysis abolished, thus once reached the maximum yields remained stable. Nevertheless, it is noteworthy that when an identical experiment was performed using *Tx*Abf operating at pD 4.6 (i.e. approximately at the pK_a of the nucleophile residue), although *p*NP-α-L-Ara*f* consumption was impaired, secondary hydrolysis was conserved (Supplementary Fig. 4), indicating that the hydrolytic behavior of N344P and N344Y cannot be solely attributed to changes in the ionization state in the active site.

3.5. pH-dependent inhibition mediated by the leaving group

As well as being pH dependent, the catalytic behavior of the mutants N344P or Y also appeared to be tightly correlated with *p*NP-α-L-Ara*f*

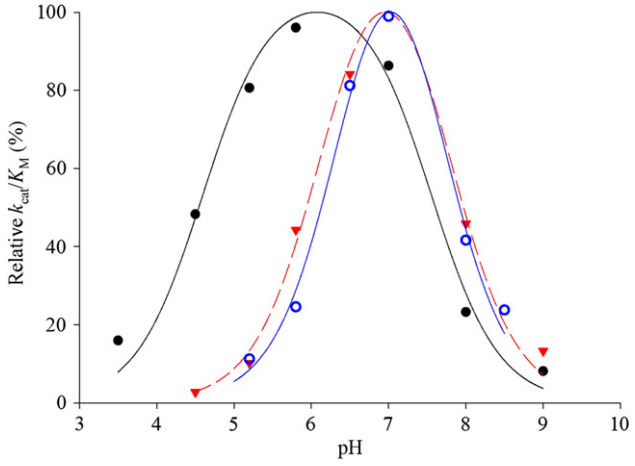

Fig. 4. pH dependency of k_{cat}/K_M for *Tx*Abf (●, solid black), N344P (▼, dashed red) and N344Y (○, solid blue). For each enzyme, the relative k_{cat}/K_M represents a percentage of the maximum $(k_{cat}/K_M)_{max}$ obtained from the theoretical model, for experimental (symbols) and model-fitted points (lines).

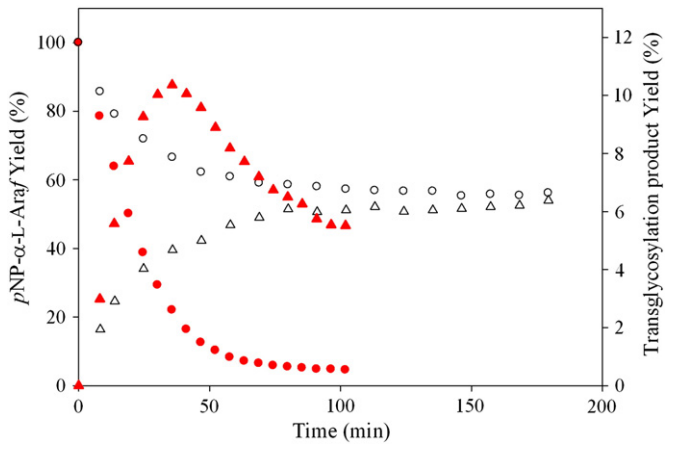

Fig. 5. Time-course NMR monitoring of A^3XX transglycosylation product (5.32 ppm) (△ and ▲ for pD 5.9 and 7.1, respectively) obtained by transglycosylation reaction catalyzed by N344Y (419 nM), with *p*NP-α-L-Ara*f* (5 mM) as donor (○ and ●, respectively) and xylotriose (10 mM) as acceptor. Assays were conducted in 25 mM deuterated sodium acetate (pD 5.9) or phosphate (pD 7.1) buffer, in D_2O, at 45 °C.

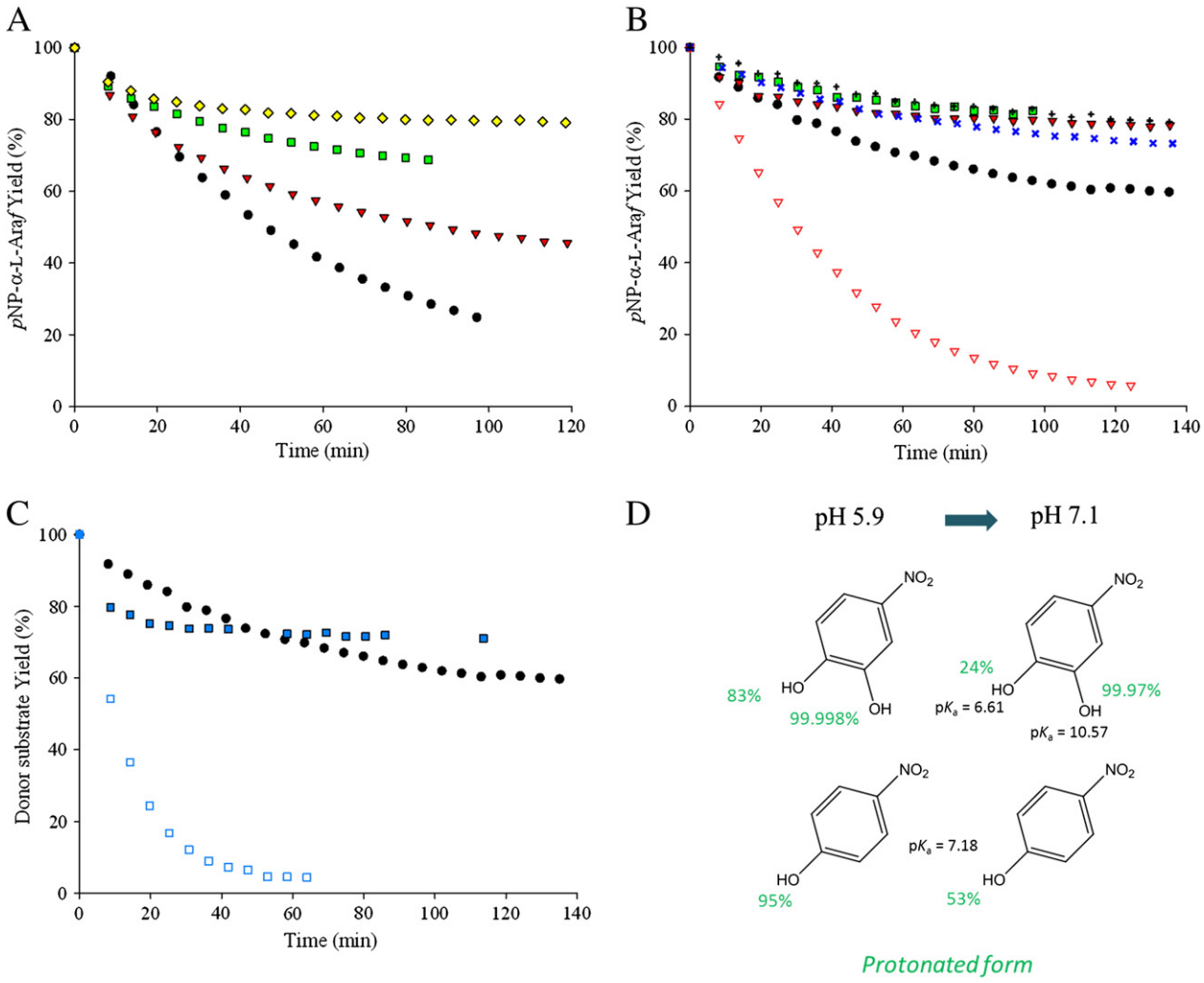

Fig. 6. Leaving group inhibition analysis of N344Y. The consumption of *p*NP-α-L-Ara*f*, monitored using ^{1}H NMR, was performed at pD 5.9 using different initial concentrations of *p*NP (0 mM, ●; 2 mM, ▼; 5 mM, ■; and 7.5 mM, ◆) and (A) 250 nM of N344Y or (B) double N344Y concentration (500 nM), revealing weaker inhibition effect. (A) The protonated form of *p*NP is not responsible for inhibition as shown by the progress curve performed at pD 7.1 (▽) with 1.9 mM of protonated *p*NP (53% of 3.55 mM initial *p*NP concentration) as opposed to 1.9 mM protonated *p*NP at pD 5.9 (▼, 95% of 2 mM initial *p*NP concentration). The leaving group hydroxyl position does not drastically modifies the inhibition profile as highlighted by *p*NP-α-L-Ara*f* (5 mM) consumption in presence of 5 mM of *o*NP (×) or *m*NP (+). (C) An extra vicinal hydroxyl does not alleviate the inhibition as shown by the reaction carried out with 4NTC-α-L-Ara*f* (5 mM) as donor substrate at pD 5.9 (■) and does not prevent enzyme 'reactivation' at pD 7.1 (□), compared to 5 mM of *p*NP (●). pH dependence inhibition assays were conducted in 25 mM deuterated acetate (pD 5.9) or phosphate (pD 7.1) buffer, at 45 °C. (D) Percentage of leaving group protonated form.

decomposition, since maximum transglycosylation yield was reached at approximately the point at which donor consumption ceased. Regarding, the premature endpoint of the reaction, it seemed likely that this be the result of concentration-dependent product inhibition. Performing reactions in the presence of various concentrations of *p*NP quickly confirmed this hypothesis (Fig. 6A) revealing a competitive inhibition that could be partly alleviated at pD 5.9 by adding more enzyme (Fig. 6B). Being pH-dependent, inhibition was fully alleviated at pD 7.1, although this did not appear to be linked to the protonation state of *p*NP, or the relative positions of the hydroxyl and nitro groups. Indeed, the use of other related compounds displaying different pK_a values and structures, such as *o*NP, *m*NP and 4-nitrocatechol (4NTC), provided very similar results (Fig. 6B–D).

3.6. Enzyme-substrates/products recognition and interactions

Taking into account the fact that the R_T of L-Ara*f* are increased in reactions catalyzed by mutants N344P and Y, enzyme-substrate and enzyme-product interactions were studied to better understand their role in the T/H partition. Monitoring the release of *p*NP from *p*NP-α-L-Ara*f* in presence of 10 mM of xylobiose revealed that *Tx*Abf was inhibited, with a relative activity of 73%, compared to the same reaction performed in the absence of acceptor [45]. However, N344P and Y did not display this property since, in the presence of an identical concentration of xylobiose, relative activities were slightly increased to 105 and 117% respectively (Supplementary Table 3). Therefore, to determine whether the modified T/H ratios of reactions catalyzed by the N344 mutants modification entail alterations in donor and/or transglycosylation product recognition, Saturation Transfer Difference (STD) NMR was employed to probe substrate-associated proton: enzyme interactions. To achieve this, inactivated enzymes, *Tx*Abf, N344G, N344P and N344Y, were prepared and used. Measurement of the residual activities of the various inactivated enzymes confirmed that, in the conditions of the STD NMR experiments, all were sufficiently inactive on *p*NP-α-L-Ara*f* (*Tx*Abf, 0.039 ± 0.003; N344G, 0.015 ± 0.001; N344P, 0.014 ± 0.002 and N344Y, 0.0030 ± 0.0003 IU.mg^{-1}), even though slight, but insignificant, modifications of the anomeric proton (H-1) signal were detected (Fig. 7A). Regarding the interaction of *p*NP-α-L-Ara*f* with the mutants, examination of the STD effects of the different protons, normalized using the STD effects measured for *Tx*Abf (i.e. I_{STD}/I_0), revealed that interactions were globally less strong, consistent with K_M values (Fig. 7B and Table 1). Even more strikingly,

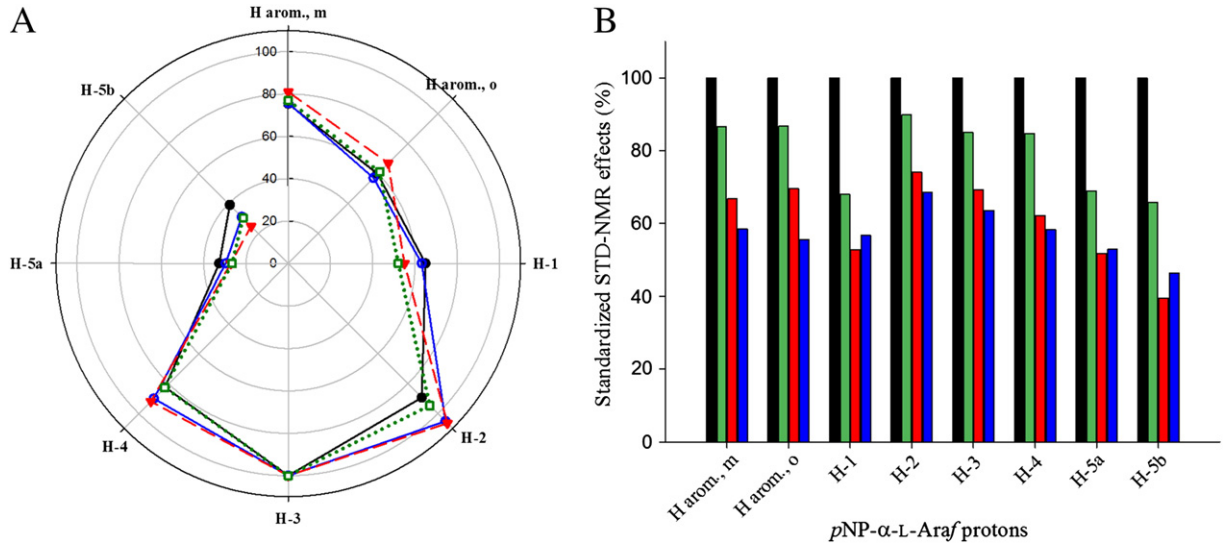

Fig. 7. STD NMR analysis of enzyme-ligand interactions. (A) STD NMR effect fingerprinting, expressed for each enzyme-ligand couple as relative percentages of the H-3 STD effect (100%), between *p*NP-α-L-Ara*f* protons and the inactivated *Tx*Abf$^+$ (●, solid black), N344G$^+$ (□, dotted green), N344P$^+$ (▼, dashed red) and N344Y$^+$ (●, solid blue). (B) Standardized STD NMR effects expressed, for each proton, as relative percentages of the effect measured between *p*NP-α-L-Ara*f* protons and the inactivated *Tx*Abf$^+$ (black) for N344G$^+$ (green), N344P$^+$ (red) and N344Y$^+$ (blue).

when the STD effects characterizing the interaction of the different mutants with A^{3}X and XA^{3}XX were measured, the I_{STD}/I_0 values of those protons that could be clearly isolated within the spectra were significantly lowered, indicating that the affinities of the mutants for such compounds are largely inferior to those for *p*NP-α-L-Ara*f*. When using A^{3}X or XA^{3}XX, the enzyme:ligand ratio was maintained at 1:100 (i.e. the same as in experiments conducted using *p*NP-α-L-Ara*f*), but the concentrations of the enzyme and ligand were increased 20-fold to maintain a constant bound enzyme concentration and obtain equivalent STD effects. Consequently, one can postulate that the value of the dissociation constant (k_{-1}/k_1) might be higher for A^{3}X and XA^{3}XX when compared to the previously reported value for *p*NP-α-L-Ara*f* ($K_d = 0.16$ mM) [65].

Beyond the comparison of the absolute STD effects of mutants with *Tx*Abf, it was also considered interesting to perform a comparative analysis of binding patterns, using internal normalization of STD signals. Accordingly, considering the proton signals of the L-Ara*f* moiety of each AXOS (i.e. H-1, H-2/H-4 and H-3 for A^{3}X and H-1, H-2 and H-4 for XA^{3}XX), no major differences were observed between inactivated mutants and *Tx*Abf (Supplementary Fig. 6). For example, considering the STD intensities of H-1 XA^{3}XX relative to H-2 XA^{3}XX (arbitrarily set to 100%) were 87, 91 and 93% for *Tx*Abf, N344P and N344Y, respectively. Similarly, the STD intensities of H-1 A^{3}X relative to H-3 A^{3}X, these were 71, 73, 72 and 77% for *Tx*Abf, N344G, N344P and N344Y, respectively. Significantly, these interactions are higher than those observed for H-1 *p*NP-α-L-Ara*f* relative to H-2 or H-3 *p*NP-α-L-Ara*f* (73 and 65% for *Tx*Abf, 55 and 52 for N344G, 52 and 55% for N344P and 60 and 63% for N344Y, respectively). Consequently, although N344 mutants do not alter the overall STD fingerprints of the donor, or of compounds representative of transglycosylation products, it would appear that the interaction of the L-Ara*f* moiety with the enzymes is different depending on the nature of the groups occupying the acceptor subsite(s). Unfortunately, the complexity of the NMR spectra recorded for A^{3}X and XA^{3}XX precluded any STD analyses of interactions with the D-xylopyranosyl moieties.

4. Discussion

In previous work on *Tx*Abf, several active site residues have been shown to be important for hydrolytic activity [65,66]. However, to predict what the role of these, or that of other residues, could be in determining the T/H partition is not yet feasible, since our current understanding of this phenomenon is insufficient. Indeed, this remark holds true for all GHs, thus the option of using directed evolution to pinpoint pertinent residues for further investigation is an adequate, albeit opportunist, approach. In our previous work we have done just this, applying a screening strategy that is powerful enough to isolate mutants that have an apparent increased activity in the presence of acceptor sugars [45]. Having isolated mutants, the selection of clones for this study, specifically displaying substitutions at position 344, was based on a three-point argumentation: the repeated occurrence of mutations at position 344, even in two separate libraries, the relatively conserved nature of N344 in GH51 and, finally, the location of N344 in a second shell, close to the nucleophile catalytic residue E298. Taken separately these criteria may not have justified our study, but together they constitute a rather interesting starting point.

4.1. Why do mutations at position 344 alter the ionization state of the catalytic nucleophile?

Like many other GHs, *Tx*Abf catalyzes both the hydrolysis and the formation of glycosidic bonds via the well-known, two-step displacement mechanism described by D. Koshland [67]. This mechanism involves two amino acids bearing carboxylic acids, one acting as the general acid/base and the other as the nucleophile, the latter being deprotonated at the start of the reaction (Fig. 1). Accordingly, it is possible to affirm that the optimum pH for the activity of *Tx*Abf is related to two pK_a values, the higher being attributed to the acid/base (E176) and the lower one to the nucleophile (E298). Nevertheless, these pK_a values are actually apparent pK_a, since the active site can be better considered as a 'polyprotic acid', because of the extensive hydrogen bonding network. The unusually high pK_a value for the acid/base amino acid in GHs is illustrative of this point, since free carboxylic acid functions display pK_a values < 5. However, in the case of the acid/base, its pK_a is strongly influenced by the nucleophilicity of the neighboring (within approximately 5 Å) catalytic nucleophile. In this study, the pK_a values measured for *Tx*Abf are quite similar to those obtained in others studies, conducted for example on a β-xylosidase (GH52) [64] or a xylanase (GH11) [37], and in general terms are consistent with the expected values for a GH. Importantly, these pK_a values were determined from experimental k_{cat}/K_M data points, thus they reflect the ionization states of the catalytic residues of unbound *Tx*Abf, meaning that the

impact of mutations at position 344 is substrate independent. Accordingly, the modified optimum pH of the mutants N344P and Y is essentially due to an increased pK_a value for E298, which means that the fraction of appropriately charged E298 is decreased at pH 5.8. In order to understand how N344 modulates the 'nucleophilic strength' of E298, it is important to note that N344 is located on strand β8, which underlies the strand β7 bearing E298 (Fig. 2A). From this location it is highly probable that N344 participates in a hydrogen bonding network that includes E298.

4.2. Why do mutations at position 344 alter the turnover number?

In this work, we have shown that mutations at position 344 affected all of the Michaelis–Menten parameters. One explanation for these overarching effects could be that glycosidic bond cleavage step and leaving group departure (k_2) are affected, which is consistent with alteration of the ionization state of the catalytic residues and the observed drastic decrease of the k_{cat}/K_M values for N344P and Y. Nevertheless, the finding that solvent KIE values (i.e. H_2O versus D_2O activation/attack) for both N344 mutants and *Tx*Abf were > 1 suggests that deglycosylation (k_3) remains rate-limiting. Moreover, accounting for the fact that the solvent KIE values for N344P and *Tx*Abf were rather similar, it is logical to assume that the decreased k_{cat}/K_M value is due to a lowered k_2 value (leaving group departure), underlining the fact that the formation or disruption of the glycosyl-enzyme E298-C1(L-Ara*f*) bond has become a critical chemical step. Nevertheless, for N344Y a slight increase in the solvent KIE value was observed, which is possibly indicative of modifications to both k_2 and k_3.

4.3. The pH-dependent character of the catalytic properties of 344 mutants

Interestingly, when reactions catalyzed by N344P or Y mutants were performed at their optimum pH, both primary and secondary hydrolysis were restored, revealing that these enzymes are highly sensitive to the ionization state in the active site. This is apparently not the case for *Tx*Abf, which conserves hydrolytic activity, albeit no longer optimal, upon pH changes. This observation is probably indicative of a breakdown of the original hydrogen bond network in the mutants, which underpins normal, quite robust hydrolytic activity.

With regard to transglycosylation, when the optimum pH for the mutants is selected, the yield of transglycosylation products is increased. This can be partly explained by the fact that transglycosylation is under kinetic control, thus in the initial phase of the *Tx*Abf-catalyzed reaction, the concentration of transglycosylation products increases progressively within a general context of high donor concentration. However, at a certain point the donor concentration falls below a critical level, while transglycosylation simultaneously attains a critical high level, thus provoking secondary hydrolysis, which targets the transglycosylation product(s). In the case of the mutants, as mentioned above, the pH shift towards optimum pH partially restores hydrolysis, probably by providing adequate conditions for the acid/base to adopt its basic form, a requirement for the activation of incoming acceptors (water or sugar molecules). The pH shift also alleviates enzyme inhibition, which is somehow mediated by the *p*NP product, although the exact nature of the inhibition is unknown. Our results indicate that the protonated species is not the inhibitor and, because inhibition was observed at pH 5.8 (i.e. more than 1 log unit under the pK_a value of *p*NP), one can exclude *p*-nitrophenolate as the inhibitory species too. Furthermore, because the different nitrophenols (*p*NP, *o*NP and *m*NP), and even 4NTC, provoked similar inhibitory effects, it seems probable that this phenomenon is driven by an enzyme-product interaction that involves the phenyl ring, maybe via modified stacking interactions. In GHs that are subject to product inhibition, loop movements are sometimes involved [68,69]. Regarding *Tx*Abf, at least one significant loop movement has been shown to be involved in catalysis [65,66], thus pH-dependent protein dynamics could well be the basis for inhibition, but further work needs to be done to investigate this.

4.4. What are the underlying reasons for the improved transglycosylation ability of the mutants?

The use of xylobiose as acceptor appeared to slightly activate mutants N344P and Y, procuring higher activity compared to *Tx*Abf, which is actually inhibited (Supplementary Table 3). This observation is consistent with the fact that in reactions where the natural acceptor is used, the T/H ratio is more in favor of glycosynthesis. Nevertheless, STD NMR experiments did not provide any evidence that would support an alteration in donor positioning in subsite −1, the binding map being similar for *Tx*Abf and the mutants. Therefore, taking into account the k_{cat}/K_M drastic decrease, it is more likely that increased transglycosylation can be explained by thermodynamics, and more specifically regarding the transition state energy barriers associated with the formation of the glycosyl-enzyme intermediate (k_2) and/or deglycosylation step (k_3). In this case, we postulate that, for N344P and N344Y, an increase in the transition state energy barrier during the glycosylation step (ΔE_a can be approximated by $-RT.\ln[(k_{cat}/K_M)_{mut}/(k_{cat}/K_M)_{wt}] = 1.9$ and 2.6 kcal.mol^{-1}, respectively) must be mirrored by a similar perturbation in the deglycosylation step. To explain this, we suppose that changes in the properties of the oxycarbenium intermediate transition state (TS2) in the mutants make water-mediated deglycosylation unfavorable and that, on the other hand, greater interactions provided by a sugar acceptor (relative to a single water molecule) lower the energy level of acceptor-mediated deglycosylation transition state, and increase the T/H ratio. In the mutants N344P and Y, acceptor-mediated activation (assessed by monitoring *p*NP release) is actually very low compared to the apparent increase in R_T. Therefore, it is likely that the mutations do not actually alleviate inhibition, but rather render acceptor-mediated deglycosylation advantageous to surmount the energy barrier.

In addition to the competition between water and non-water acceptor molecules, which determines the outcome of the deglycosylation step, the overall transglycosylation yield is also determined by the half-life of the product, which can be increased by reducing the enzyme's ability to hydrolyze it. To achieve this, it is important to take into account the fact that the first stage of the reaction uses an activated donor, bearing a *p*NP, which displays much higher leaving group ability than the xylobiosyl or xylotriosyl moieties present in the transglycosylation products. Considering both the k_{cat}/K_M and KIE values reported here, it appears that the mutants display diminished ability to cleave glycosidic bonds linking two sugar moieties.

5. Conclusions

In this work, we have shown that the mutants N344P and Y display a severely reduced ability to perform secondary hydrolysis, thus allowing the yield of transglycosylation products to attain a stable plateau over time. This indicates that the T/H equilibrium governing the mutant-catalyzed reactions might be modified. To our knowledge this report constitutes a first of a kind demonstration of a strategy that might be applicable to other GHs, providing that pK_a modulating residues, equivalent to N344, can be identified. Moreover, it is pertinent to wonder to what extent the mutants described in this study could be further improved. Given the fact that mutants N344P and Y lead to persistent transfuranosylation products compared to the wild-type, it might be feasible to use directed evolution to introduce other features that enhance the usefulness of *Tx*Abf as a tool for chemo-enzymatic syntheses.

Competing interests

The authors declare they have no competing interests.

Acknowledgements

PhD fellowship of B. Bissaro was supported by the Institut National de la Recherche Agronomique (INRA) [CJS]. MetaToul (Metabolomics & Fluxomics Facitilies, Toulouse, France, www.metatoul.fr) and its staff members are gratefully acknowledged for technical support and access to NMR facility. MetaToul is supported by grants from the Région Midi-Pyrénées, the European Regional Development Fund, the SICOVAL, the Infrastructures en Biologie Sante et Agronomie (IBiSa, France), the Centre National de la Recherche Scientifique (CNRS) and the Institut National de la Recherche Agronomique (INRA). STD NMR experiments were performed at the 'Integrated Screening Platform of Toulouse' (PICT, IPBS, CNRS–Université de Toulouse) using equipment funded by the French Research Ministry, CNRS, Université Paul Sabatier, the Région Midi-Pyrénées and European structural funds.

Appendix A. Supplementary data

Supplementary data to this article can be found online at http://dx.doi.org/10.1016/j.bbagen.2013.10.013.

References

[1] R. Fauré, C.M. Courtin, J.A. Delcour, C. Dumon, C.B. Faulds, G.B. Fincher, S. Fort, S.C. Fry, S. Halila, M.A. Kabel, L. Pouvreau, B. Quemener, A. Rivet, L. Saulnier, H.A. Schols, H. Driguez, M.J. O'Donohue, A brief and informationally rich naming system for oligosaccharide motifs of heteroxylans found in plant cell walls, Aust. J. Chem. 62 (2009) 533–537.
[2] J. Kadokawa, Precision polysaccharide synthesis catalyzed by enzymes, Chem. Rev. 111 (2011) 4308–4345.
[3] R. Kittl, S.G. Withers, New approaches to enzymatic glycoside synthesis through directed evolution, Carbohydr. Res. 345 (2010) 1272–1279.
[4] B. Rakić, S.G. Withers, Recent developments in glycoside synthesis with glycosynthases and thioglycoligases, Aust. J. Chem. 62 (2009) 510–520.
[5] R.M. Schmaltz, S.R. Hanson, C.-H. Wong, Enzymes in the synthesis of glycoconjugates, Chem. Rev. 111 (2011) 4259–4307.
[6] C. Dumon, L. Song, S. Bozonnet, R. Fauré, M.J. O'Donohue, Progress and future prospects for pentose-specific biocatalysts in biorefining, Process Biochem. 47 (2012) 346–357.
[7] B. Tefsen, A.F.J. Ram, I. van Die, F.H. Routier, Galactofuranose in eukaryotes: aspects of biosynthesis and functional impact, Glycobiology 22 (2012) 456–469.
[8] M. Oppenheimer, A.L. Valenciano, P. Sobrado, Biosynthesis of galactofuranose in kinetoplastids: novel therapeutic targets for treating leishmaniasis and chagas' disease, Enzyme Res. 2011 (2011) 1–13.
[9] L.L. Pedersen, S.J. Turco, Cellular and molecular life sciences galactofuranose metabolism: a potential target for antimicrobial chemotherapy, Cell. Mol. Life Sci. 60 (2003) 259–266.
[10] L.F. Mackenzie, Q. Wang, R.A.J. Warren, S.G. Withers, Glycosynthases: mutant glycosidases for oligosaccharide synthesis, J. Am. Chem. Soc. 120 (1998) 5583–5584.
[11] N.N. Aronson, B.A. Halloran, M.F. Alexeyev, X.E. Zhou, Y. Wang, E.J. Meehan, L. Chen, Mutation of a conserved tryptophan in the chitin-binding cleft of *Serratia marcescens* chitinase A enhances transglycosylation, Biosci. Biotechnol. Biochem. 70 (2006) 243–251.
[12] H. Mori, K.S. Bak-Jensen, B. Svensson, Barley α-amylase Met53 situated at the high-affinity subsite −2 belongs to a substrate binding motif in the β → α loop 2 of the catalytic $(\beta/\alpha)_8$-barrel and is critical for activity and substrate specificity, Eur. J. Biochem. 269 (2002) 5377–5390.
[13] S. Armand, S.R. Andrews, S.J. Charnock, H.J. Gilbert, Influence of the aglycone region of the substrate binding cleft of *Pseudomonas* xylanase 10A on catalysis, Biochemistry 40 (2001) 7404–7409.
[14] S.-Q. Fan, W. Huang, L.-X. Wang, Remarkable transglycosylation activity of glycosynthase mutants of endo-D, an endo-β-*N*-acetylglucosaminidase from *Streptococcus pneumoniae*, J. Biol. Chem. 287 (2012) 11272–11281.
[15] H.-Y. Feng, J. Drone, L. Hoffmann, V. Tran, C. Tellier, C. Rabiller, M. Dion, Converting a β-glycosidase into a β-transglycosidase by directed evolution, J. Biol. Chem. 280 (2005) 37088–37097.
[16] A. Moreau, F. Shareck, D. Kluepfel, R. Morosoli, Alteration of the cleavage mode and of the transglycosylation reactions of the xylanase A of *Streptomyces lividans* 1326 by site-directed mutagenesis of the Asn173 residue, Eur. J. Biochem. 219 (1994) 261–266.
[17] T. Taira, M. Fujiwara, N. Dennhart, H. Hayashi, S. Onaga, T. Ohnuma, T. Letzel, S. Sakuda, T. Fukamizo, Transglycosylation reaction catalyzed by a class V chitinase from cycad, *Cycas revoluta*: A study involving site-directed mutagenesis, HPLC, and real-time ESI-MS, Biochim. Biophys. Acta Proteins Proteomics 1804 (2010) 668–675.
[18] M. Umekawa, W. Huang, B. Li, K. Fujita, H. Ashida, L.-X. Wang, K. Yamamoto, Mutants of *Mucor hiemalis* endo-β-*N*-acetylglucosaminidase show enhanced transglycosylation and glycosynthase-like activities, J. Biol. Chem. 283 (2008) 4469–4479.
[19] M.A. Frutuoso, S.R. Marana, A single amino acid residue determines the ratio of hydrolysis to transglycosylation catalyzed by β-glucosidases, Protein Pept. Lett. 20 (2013) 102–106.
[20] M. Hidaka, S. Fushinobu, Y. Honda, T. Wakagi, H. Shoun, M. Kitaoka, Structural explanation for the acquisition of glycosynthase activity, J. Biochem. 147 (2010) 237–244.
[21] Y. Honda, S. Fushinobu, M. Hidaka, T. Wakagi, H. Shoun, H. Taniguchi, M. Kitaoka, Alternative strategy for converting an inverting glycoside hydrolase into a glycosynthase, Glycobiology 18 (2008) 325–330.
[22] T. Kuriki, H. Kaneko, M. Yanase, H. Takata, J. Shimada, S. Handa, T. Takada, H. Umeyama, S. Okada, Controlling substrate preference and transglycosylation activity of neopullulanase by manipulating steric constraint and hydrophobicity in active center, J. Biol. Chem. 271 (1996) 17321–17329.
[23] R. Kuroki, L.H. Weaver, B.W. Matthews, Structural basis of the conversion of T4 lysozyme into a transglycosidase by reengineering the active site, Proc. Natl. Acad. Sci. U. S. A. 96 (1999) 8949–8954.
[24] C. Giacomini, G. Irazoqui, P. Gonzalez, F. Batista-viera, B.M. Brena, Enzymatic synthesis of galactosyl–xylose by *Aspergillus oryzae* β-galactosidase, J. Mol. Catal. B Enzym. 20 (2002) 159–165.
[25] S. Malá, H. Dvoráková, R. Hrabal, B. Králová, Towards regioselective synthesis of oligosaccharides by use of α-glucosidases with different substrate specificity, Carbohydr. Res. 322 (1999) 209–218.
[26] M. Ribeirão, V.L. Pereira-Chioccola, D. Eichinger, M.M. Rodrigues, S. Schenkman, Temperature differences for *trans*-glycosylation and hydrolysis reaction reveal an acceptor binding site in the catalytic mechanism of *Trypanosoma cruzi trans*-sialidase, Glycobiology 7 (1997) 1237–1246.
[27] E. Bonnin, J. Vigouroux, Kinetic parameters of hydrolysis and transglycosylation catalyzed by an exo-β-(1,4)-galactanase, Enzyme Microb. Technol. 20 (1997) 516–522.
[28] G. Perugino, A. Trincone, A. Giordano, J. van der Oost, T. Kaper, M. Rossi, M. Moracci, Activity of hyperthermophilic glycosynthases is significantly enhanced at acidic pH, Biochemistry 42 (2003) 8484–8493.
[29] A. Trincone, A. Giordano, G. Perugino, M. Rossi, M. Moracci, Glycosynthase-catalysed syntheses at pH below neutrality, Bioorg. Med. Chem. Lett. 13 (2003) 4039–4042.
[30] M. Hrmova, T. Imai, S.J. Rutten, J.K. Fairweather, V. Bulone, H. Driguez, G.B. Fincher, Mutated barley (1,3)-β-D-glucan endohydrolases synthesize crystalline (1,3)-β-D-glucans, J. Biol. Chem. 277 (2002) 30102–30111.
[31] M. Pérez-Sánchez, Á. Cortés Cabrera, H. García-Martín, J.V. Sinisterra, J.I. García, M.J. Hernáiz, Improved synthesis of disaccharides with *Escherichia coli* β-galactosidase using bio-solvents derived from glycerol, Tetrahedron 67 (2011) 7708–7712.
[32] L.P. McIntosh, G. Hand, P.E. Johnson, M.D. Joshi, M. Ko, L.A. Plesniak, L. Ziser, W.W. Wakarchuk, S.G. Withers, The pK_a of the general acid/base carboxyl group of a glycosidase cycles during catalysis: A ^{13}C-NMR study of *Bacillus circulans* xylanase, Biochemistry 35 (1996) 9958–9966.
[33] C. Malet, A. Planas, Mechanism of *Bacillus* 1,3-1,4-β-D-glucan 4-glucanohydrolases: kinetics and pH studies with 4-methylumbelliferyl β-D-glucan oligosaccharides, Biochemistry 36 (1997) 13838–13848.
[34] K. Bartik, C. Redfield, C.M. Dobson, Measurement of the individual pK_a values of acidic residues of hen and turkey lysozymes by two-dimensional ^{1}H NMR, Biophys. J. 66 (1994) 1180–1184.
[35] D.L. Zechel, S.G. Withers, Dissection of nucleophilic and acid–base catalysis in glycosidases, Curr. Opin. Chem. Biol. 5 (2001) 643–649.
[36] A. Vasella, G.J. Davies, M. Böhm, Glycosidase mechanisms, Curr. Opin. Chem. Biol. 6 (2002) 619–629.
[37] M.D. Joshi, G. Sidhu, J.E. Nielsen, G.D. Brayer, S.G. Withers, L.P. McIntosh, Dissecting the electrostatic interactions and pH-dependent activity of a family 11 glycosidase, Biochemistry 40 (2001) 10115–10139.
[38] M.D. Joshi, G. Sidhu, I. Pot, G.D. Brayer, S.G. Withers, L.P. McIntosh, Hydrogen bonding and catalysis: a novel explanation for how a single amino acid substitution can change the pH optimum of a glycosidase, J. Mol. Biol. 299 (2000) 255–279.
[39] M.L. Ludwiczek, I. D'Angelo, G.N. Yalloway, J. Brockerman, M. Okon, J.E. Nielsen, N.C.J. Strynadka, S.G. Withers, L.P. McIntosh, Strategies for modulating the pH-dependent activity of a family 11 glycoside hydrolase, Biochemistry 52 (2013) 3138–3156.
[40] C. Rémond, R. Plantier-Royon, N. Aubry, E. Maes, C. Bliard, M.J. O'Donohue, Synthesis of pentose-containing disaccharides using a thermostable α-L-arabinofuranosidase, Carbohydr. Res. 339 (2004) 2019–2025.
[41] C. Rémond, R. Plantier-Royon, N. Aubry, M.J. O'Donohue, An original chemoenzymatic route for the synthesis of β-D-galactofuranosides using an α-L-arabinofuranosidase, Carbohydr. Res. 340 (2005) 637–644.
[42] R. Euzen, G. Lopez, C. Nugier-Chauvin, V. Ferrières, D. Plusquellec, C. Rémond, M. O'Donohue, A chemoenzymatic approach for the synthesis of unnatural disaccharides containing D-galacto or D-fucofuranosides, Eur. J. Org. Chem. 2005 (2005) 4860–4869.
[43] G. Lopez, C. Nugier-Chauvin, C. Rémond, M. O'Donohue, Investigation of the specificity of an α-L-arabinofuranosidase using C-2 and C-5 modified α-L-arabinofuranosides, Carbohydr. Res. 342 (2007) 2202–2211.
[44] F. Arab-Jaziri, B. Bissaro, M. Dion, O. Saurel, D. Harrison, F. Ferreira, A. Milon, C. Tellier, M.J. O'Donohue, R. Fauré, Engineering transglycosidase activity into a GH51 α-L-arabinofuranosidase, New Biotechnol. 30 (2013) 536–544.
[45] F. Arab-Jaziri, B. Bissaro, C. Tellier, M. Dion, R. Fauré, M.J. O'Donohue, Enhancing the chemoenzymatic synthesis of arabinosylated xylo-oligosaccharides by GH51 α-L-arabinofuranosidase using a directed evolution approach, Unpublished results.
[46] C. Rémond, M. Ferchichi, N. Aubry, R. Plantier-Royon, C. Portella, M.J. O'Donohue, Enzymatic synthesis of alkyl arabinofuranosides using a thermostable α-L-arabinofuranosidase, Tetrahedron Lett. 43 (2002) 9653–9655.
[47] L. Marmuse, M. Asther, E. Fabre, D. Navarro, L. Lesage-Meessen, M. Asther, M. O'Donohue, S. Fort, H. Driguez, New chromogenic substrates for feruloyl esterases, Org. Biomol. Chem. 6 (2008) 1208–1214.
[48] H. Gruppen, R.A. Hoffmann, F.J. Kormelink, A.G. Voragen, J.P. Kamerling, J.F. Vliegenthart, Characterisation by ^{1}H NMR spectroscopy of enzymically derived

oligosaccharides from alkali-extractable wheat-flour arabinoxylan, Carbohydr. Res. 233 (1992) 45–64.
[49] J.J. Ordaz-Ortiz, F. Guillon, O. Tranquet, G. Dervilly-Pinel, V. Tran, L. Saulnier, Specificity of monoclonal antibodies generated against arabinoxylans of cereal grains, Carbohydr. Polym. 57 (2004) 425–433.
[50] M. Vrsanská, W. Nerinckx, M. Claeyssens, P. Biely, An alternative approach for the synthesis of fluorogenic substrates of *endo*-β-(1 → 4)-xylanases and some applications, Carbohydr. Res. 343 (2008) 541–548.
[51] R.A. Hoffman, B.R. Leeflang, M.M.J. de Barse, J.P. Kamerling, J.F.G. Vliegenthart, Characterisation by ^{1}H-NMR spectroscopy of oligosaccharides, derived from arabinoxylans of white endosperm of wheat, that contain the elements → 4)[α-L-Ara*f*-(1 → 3)]-β-D-Xyl*p*-(1 → or → 4)[α-L-Ara*f*-(1 → 2)][α-L-Ara*f*-(1 → 3)]-β-D-Xyl*p*-(1→, Carbohydr. Res. 221 (1991) 63–81.
[52] T. Debeche, N. Cummings, I. Connerton, P. Debeire, M.J. O'Donohue, Genetic and biochemical characterization of a highly thermostable α-L-arabinofuranosidase from *Thermobacillus xylanilyticus*, Appl. Environ. Microbiol. 66 (2000) 1734–1736.
[53] H.E. Gottlieb, V. Kotlyar, A. Nudelman, NMR chemical shifts of common laboratory solvents as trace impurities, J. Org. Chem. 3263 (1997) 7512–7515.
[54] P.K. Glasoe, F.A. Long, Use of glass electrodes to measure acidities in deuterium oxide, J. Phys. Chem. 64 (1960) 188–190.
[55] R.J. Vietor, R.A. Hoffmann, S.A.G.F. Angelino, A.G.J. Voragen, J.P. Kamerling, J.F.G. Vliegenthart, Structures of small oligomers liberated from barley arabinoxylans by endoxylanase from *Aspergillus awamori*, Carbohydr. Res. 254 (1994) 245–255.
[56] H. Ferré, A. Broberg, J.O. Duus, K.K. Thomsen, A novel type of arabinoxylan arabinofuranohydrolase isolated from germinated barley analysis of substrate preference and specificity by nano-probe NMR, Eur. J. Biochem. 267 (2000) 6633–6641.
[57] H. Pastell, P. Tuomainen, L. Virkki, M. Tenkanen, Step-wise enzymatic preparation and structural characterization of singly and doubly substituted arabinoxylo-oligosaccharides with non-reducing end terminal branches, Carbohydr. Res. 343 (2008) 3049–3057.
[58] L. Pitkänen, P. Tuomainen, L. Virkki, M. Tenkanen, Molecular characterization and solution properties of enzymatically tailored arabinoxylans, Int. J. Biol. Macromol. 49 (2011) 963–969.
[59] M.A.S. Correia, K. Mazumder, J.L.A. Brás, S.J. Firbank, Y. Zhu, R.J. Lewis, W.S. York, C.M.G.A. Fontes, H.J. Gilbert, Structure and function of an arabinoxylan-specific xylanase, J. Biol. Chem. 286 (2011) 22510–22520.
[60] M. Mayer, B. Meyer, Group epitope mapping by saturation transfer difference NMR to identify segments of a ligand in direct contact with a protein receptor, J. Am. Chem. Soc. 123 (2001) 6108–6117.
[61] D. Shallom, V. Belakhov, D. Solomon, G. Shoham, T. Baasov, Y. Shoham, Detailed kinetic analysis and identification of the nucleophile in α-L-arabinofuranosidase from *Geobacillus stearothermophilus* T-6, a family 51 glycoside hydrolase, J. Biol. Chem. 277 (2002) 43667–43673.
[62] D.L. Zechel, S.G. Withers, Glycosidase mechanisms: anatomy of a finely tuned catalyst, Acc. Chem. Res. 33 (2000) 11–18.
[63] M.L. Sinnott, Catalytic mechanism of enzymic glycosyl transfer, Chem. Rev. 90 (1990) 1171–1202.
[64] T. Bravman, G. Zolotnitsky, V. Belakhov, G. Shoham, B. Henrissat, T. Baasov, Y. Shoham, Detailed kinetic analysis of a family 52 glycoside hydrolase: a β-xylosidase from *Geobacillus stearothermophilus*, Biochemistry 42 (2003) 10528–10536.
[65] F. Arab-Jaziri, B. Bissaro, S. Barbe, O. Saurel, H. Débat, C. Dumon, V. Gervais, A. Milon, I. André, R. Fauré, M.J. O'Donohue, Functional roles of H98 and W99 and β2α2 loop dynamics in the α-L-arabinofuranosidase from *Thermobacillus xylanilyticus*, FEBS J. 279 (2012) 3598–3611.
[66] G. Paës, L.K. Skov, M.J. O'Donohue, C. Rémond, J.S. Kastrup, M. Gajhede, O. Mirza, The structure of the complex between a branched pentasaccharide and *Thermobacillus xylanilyticus* GH-51 arabinofuranosidase reveals xylan-binding determinants and induced fit, Biochemistry 47 (2008) 7441–7451.
[67] D.E. Koshland Jr., Stereochemistry and the mechanism of enzymatic reactions, Biol. Rev. Camb. Philos. Soc. 28 (1953) 416–436.
[68] L. Bu, M.F. Crowley, M.E. Himmel, G.T. Beckham, Computational investigation of pH dependence on loop flexibility and catalytic function in glycoside hydrolases, J. Biol. Chem. 288 (2013) 12175–12186.
[69] V. Nahoum, G. Roux, V. Anton, P. Rougé, A. Puigserver, H. Bischoff, B. Henrissat, F. Payan, Crystal structures of human pancreatic α-amylase in complex with carbohydrate and proteinaceous inhibitors, Biochem. J. 346 (2000) 201–208.